Journal of Nuclear Medicine, published on April 13, 2018 as doi:10.2967/jnumed.117.206375

Development and validation of a rebinner with rigid motion correction for the Siemens PET/MR scanner: Application to a large cohort of ^{11}C-PIB scans.

Anthonin Reilhac[1,2], Inés Merida[2], Zacharie Irace[2] , Mary C. Stephenson[1], Ashley A. Weekes[1], Christopher Chen[3,4], John J. Totman[1], David W. Townsend[1], Hadi Fayad[5,6] and Nicolas Costes[2]

[1]Clinical Imaging Research Centre, A*STAR-NUS, Singapore.

[2]CERMEP-Imagerie du vivant, Lyon, France.

[3]Department of Pharmacology, National University of Singapore, Singapore.

[4]Memory Aging & Cognition Centre, National University Health System, Singapore.

[5]OHS, PET/CT, Hamad Medical Corporation, Doha, Qatar.

[6]LaTIM, INSERM UMR 1101, Brest, France.

Corresponding author:

Anthonin Reilhac, Ph.D.

A*STAR-NUS Clinical Imaging Research Centre

Centre for Translational Medicine (MD6)

14 Medical Drive, B1-01, Singapore 117599

E-mail: Anthonin_Reilhac@CIRC.a-star.edu.sg

Number of words: 5014

Short title: A rebinner with rigid motion correction

Conflicts of interest: None.

Financial Support: This work was supported by the French national 'invest for the future' programs (LILI Lyon Integrated Life Imaging: hybrid MR-PET ANR-11-EQPX-0026), the hospital University Institut CESAME (Brain and Mental Health ANR-10-IBHU-0003) and by France Life Imaging (FLI, ANR-11-INBS-0006). The ^{11}C-PIB study was funded by the NUHS-CG CIRC Seed Funding and by the SoM Aspiration Fund (World Class) Category.

ABSTRACT

Objective: Head motion occurring during brain PET studies leads to image blurring and to bias in measured local quantities. Our first objective was to implement an accurate list-mode-based rigid motion correction method for PET data acquired with the mMR synchronous Positron Emission Tomography/Magnetic Resonance (PET/MR) scanner. Our second objective was to optimize the correction for ^{11}C-PIB scans using simulated and actual data with well-controlled motions.

Results: An efficient list-mode based motion correction approach has been implemented, fully optimized and validated using simulated as well as actual PET data. The average spatial resolution loss induced by inaccuracies in motion parameter estimates as well as by the rebinning process was estimated to correspond to a 1 mm increase in Full Width Half Maximum (FWHM) with motion parameters estimated directly from the PET data with a temporal frequency of 20 secs. The results show that it can be safely applied to the ^{11}C-PIB scans, allowing almost complete removal of motion induced artifacts. The application of the correction method on a large cohort of ^{11}C-PIB scans led to the following observations: i) more than 21% of the scans were affected by a motion greater than 10 mm (39% for subjects with Mini-Mental State Examination -MMSE scores below 20) and ii), the correction led to quantitative changes in Alzheimer-specific cortical regions of up to 30%.

Conclusion: The rebinner allows an accurate motion correction at a cost of minimal resolution reduction. The application of the correction to a large cohort of ^{11}C-PIB scans confirmed the necessity to systematically correct for motion for quantitative results.

Keywords: PET, Rigid motion correction; list-mode rebinner, ^{11}C-PIB.

INTRODUCTION

The accuracy of Positron Emission Tomography (PET) measurements relies on the patient's ability to stay still during the data acquisition process. Head motion occurring during brain PET studies leads to image blurring, making accurate localization of structures more difficult and leads to quantitative bias in measured local quantities. In dynamic studies, patient motion alters the time activity curves, measured at each voxel or in regions of interest, and introduces errors in the parameter estimates derived from kinetic modeling. Methods to correct for head motion can be classified in two broad categories depending on whether the correction occurs during the list-mode rebinning/reconstruction step or after the reconstruction (*1*). Most of the post-reconstruction approaches rely on image registration algorithms to align each reconstructed time frame with a target, neglecting thus intra frame motion which is an obvious limitation. In addition and with the exception of a few implementations such as in (*2*), these methods do not correct for spatial misalignment between emission data and attenuation data leading to corrupted reconstructed volumes. Contrary to image registration-based correction, event-by-event correction accounts for intra-frame motion as well as for attenuation-emission mismatches and allows the user to freely define the final framing of the reconstruction image. To the best of our knowledge, the idea to correct for event mis-positioning during the rebinning step was first proposed by Menke et al (*3*). However, it is only a few years later that Bülher et al (*4*) clearly identified possible sources of artefacts that needed to be accounted for during the rebinning for accurate event-by-event correction. The few papers published since then, demonstrated for most of them the superiority of the event-by-event correction approach over image-based correction methods (*5*-*7*).

In this paper, we propose a novel implementation of a list-mode-based correction approach for PET data acquired with the mMR synchronous Positron Emission Tomography / Magnetic Resonance (PET/MR) scanner (*8*) (Siemens Healthcare GmbH, Erlangen, Germany). Using realistic Monte Carlo simulations as well as actual data with well controlled motion, we assessed its performance and optimized the whole correction protocol including the derivation of the rigid motion parameters from

the PET data only. Finally, we applied the motion correction on a large cohort of ^{11}C-PIB scans from which novel information on the impact of motion were derived.

MATERIALS AND METHODS

The developed rebinner reads chronologically the recorded events from the Siemens list-mode file, applies the estimated geometric transformations and frames the detected counts into static or dynamic sinograms that can be reconstructed with the standard reconstruction software. Motion correction parameters are stored in a text file where each line provides the time t at which a motion occurred and the corresponding 6 rigid parameters. In this work, the rigid body motion parameters were estimated from an initial dynamic reconstruction of the PET data. However motion parameters derived from simultaneously acquired MR data or using an external tracking device can also be used. The correction method was implemented under Linux Ubuntu 16.04. The source codes are freely available upon request. Note that a docker version is also available and automates correction and reconstruction on a deported e7 tools reconstruction machine running windows.

Estimation of the motion parameters

In order to measure the motion parameters, the PET data is first reconstructed using short time frames and without attenuation nor scatter correction for increased registration accuracy (*2*). The reconstruction is carried out using the standard Ordinary Poisson Ordered Subset Expectation Maximization reconstruction method (*9*) using 3 iterations and 21 subsets. By default a zoom of 2 is employed leading to volume dimensions of 172 × 172 × 127 with a voxel size of 2.09 × 2.09 × 2.03 mm^3. The 6 rigid transformation parameters that optimize the cross-correlation similarity criterion between the each data frame and a reference volume created from a selection of frames is computed. Volume registration as well as other data manipulation are performed using tools developed at the McConnell Brain Imaging Centre (*10*). For improved accuracy, the dynamic volume is smoothed by a

3D Gaussian kernel prior to the registration. Note that the minimal frame duration that still allows the collection of enough counts for accurate motion estimation depends on the counting statistics of the scan, the level of spatial smoothing as well as other characteristics such as the tracer pharmacokinetic. The relation between frame duration, smoothing strength and motion parameter accuracy is investigated in this work.

Rebinner implementation details

The rebinner reads the events from the list-mode file and applies the corresponding motion correction parameters to the equation of the corresponding Line Of Responses (LORs). The intersection of this line with the actual scanner ring allows the identification of the correct crystal pair and sinogram index. We addressed the LOR discretization issue (*4*) by spatially oversampling the scanner crystals, allowing for each LOR extra sub-crystal combinations to which the simple line transformation is then applied. This approach enables the determination of the proportion of events detected in LOR *i* to be reassigned to LOR *j*. In the following sections, OS_1 means no oversampling (simple LOR approach) while OS_n ($n > 1$) means a $n \times n$ subdivisions of each crystal (tangential × radial), leading for each LOR to n^2 direct and $n^2 - (n \bmod 2)$ oblique sub-crystal combinations. To account for normalization differences between original and correct LORs, detected counts in each LOR are first normalized by their respective normalization factors prior the LOR reassignment. Supplemental Figure 1 illustrates this rebinning process involving crystal oversampling and normalization. Events losses caused by the gaps are compensated by filling them with the neighbour counts prior performing the correction. To account for events leaving the scanner field of view due to motion, after assigning the counts to the correct sinogram bins, the rebinner multiplies the counts by the ratio of the frame duration and the time during which the corresponding LOR was not falling outside the field of view due to motion. Note that contrary to some correction approaches (*5*) our implementation does not take advantage of the extra events that are detected due to motion and simply discards them.

VALIDATION FRAMEWORK

Rebinning accuracy

We assessed the accuracy of the rebinner operating under different modes using simulated ^{18}F-FDG brain PET data with well-controlled motion. Each scan was a 600 secs list-mode acquisition generated with the PET-SORTEO Monte Carlo simulator modelling the geometry and physical characteristics of the Siemens mMR PET/MR system (*11*) and during which an acute basic rigid motion was applied at t = 200 secs. Each motion consisted of either a translation or a rotation with respect to one of the axis (from -10 to +10 mm with a step of 1 mm for the translations and from -10 to 10 degrees by step of 1 degree for the rotations). A total of 120 simulated scans with motion were generated this way using the same activity levels, numerical emission phantom and attenuation map. In addition, two reference scans were generated without motion using the same activity distribution and attenuation map and hence both reference scans only differed by the noise. Each list-mode scan was then rebinned into a single static 3D sinogram with a span of 1 and a maximum ring difference of 60 without and with motion correction using the true motion parameters. Different combinations of parameters related to the motion correction were tested: crystal oversampling with n varying from 1 (no oversampling) to 4, accounting or not for the difference in normalization factors and finally compensating or not for data losses. Finally, each sinogram was reconstructed into a 256 × 256 × 127 voxel volume (voxel size = 1.4 × 1.4 × 2.03 mm^3) with the 3D Ordinary Poisson Ordered Subset Expectation Maximization reconstruction method using 3 iterations and 21 subsets and with all corrections applied (*9*). The normalized Root Mean Square Errors (RMSE) computed between each reconstructed volume V and the reference volume R and expressed as a percentage of the Root Sum of Square (RSS) of the reference volume (nRMSE(V, R) = 100 . RMSE(V,R)/RSS(R)) was the metric used to assess the accuracy of the correction. In order to remove the differences between the corrected

and reference scan that were caused by the noise process only, the nRMSE computed between the two reference volumes was subtracted to the nRMSE. This final metric is hereafter called $nRMSE_0$.

Accuracy of motion estimates

The accuracy and precision with which the motion parameters can be estimated from an initial dynamic reconstruction were assessed using an actual 1800 secs ^{11}C-PIB list-mode scan selected from the ^{11}C-PIB study described in the following section. We generated first the corresponding static sinogram (no compression, span = 1, prompt and delay events stored in 2 different matrices), removing thus the temporal dimension. This sinogram can be seen as the one obtained from a motionless brain with the activity distribution being the time average distribution of the original scan. From this static sinogram, motion-free 1800 secs list-mode data were created with varying counting statistics using a non-parametric bootstrap approach which consisted in sampling with replacement of the prompt and delay events from the original scan (*12*). Four motion-free list-mode files were generated this way with counting statistics corresponding to 10%, 20%, 50% and 100% (designated by LM10%, LM20%, LM50% and LM100%) of the counts from the original scan. Each of these list-mode files was then rebinned into 90 frames of 20 secs each (designated by LM10%_20s, LM20%_20s, LM50%_20s and LM100%_20s). The full-statistics list-mode data (LM100%) was used to generate 3 additional dynamic scans of 30 frames of 60 secs (LM100%_60s), 12 frames of 150 secs (LM100%_150s) and 6 frames of 300 secs (LM100%_300s) respectively. Table 1 reports for each dynamic scan the number of frames, the frame duration, the total number of prompts as well as the number of net trues in the first and last frames. Finally, using the same 4 list-mode files, 7 additional dynamic sinograms were generated with the same counting statistics, except that rigid motion were included during the rebinning process using our rebinner program. The parameters and time at which the motion was included are reported in Table 2. Note that we deliberately did not impose motion that would had caused significant data loss (Tz, Rx and Ry). Those losses would have induced artefacts in the reconstructed images impacting the

registration process. Also, note that the motion times were chosen so that the motion would always occur in-between 2 frames for the all the tested framing parameters. Motion parameter files obtained with different 3D Gaussian smoothing kernel (from 0 to 28 mm in FWHM) applied on each frame prior to the registration process were then computed for each of the 7 motion-free and 7 motion-corrupted sinograms using our correction program. For each frame, the residual rigid motion parameters were computed as the difference between the estimated and true motion parameters (the latter being identity for the motion-free sinograms). The mean absolute Euclidean distance induced across time by the residual motion to a point located at a radial distance of 7 cm was computed and used as a metric to assess the accuracy of the estimated motion parameters. In addition, in order to estimate the loss of resolution caused by both the rebinning process as well as by inaccuracies in motion parameter estimates we simulated the acquisitions of a point source, originally located in the center of the field of view as well as at a radial distance of 7 cm along the x-axis, and during which the same motion parameters as above were applied (see Table 2). The reference spatial resolution for these two locations (0 cm and 7 cm) was measured similarly but without including any motion during the simulation. Each simulated list-mode file were rebinned using motion parameters estimated from the ^{11}C-PIB study (LM10%_20s to LM100%_600s scans with and without motion) and reconstructed using filtered-back projection algorithm into a 344 × 344 × 127 element volume with a voxel size of 0.21 × 0.21 × 2.03 mm^3. The FWHM value was then measured from each reconstructed image following the National Electrical Manufacturers Association procedure (*13*).

Application to an actual Hoffman phantom scan

A Hoffman brain phantom was filled with a solution of ^{18}F-FDG and placed at the center of the field of view of the scanner. A 60 mins acquisition was performed during which the phantom was manually moved at few occasions after 35 mins of motionless acquisition. Note that no attempt was made to control the nature nor the magnitude of the motion. The [30 – 60 mins] period, which

contained motion was rebinned in a single static frame with and without motion correction. Motion parameters were estimated using an initial reconstruction and the resulting volume was smoothed with a 3D Gaussian kernel of 16 mm (FWHM). Different framing parameters were tested (frame numbers x duration in secs): 45Fx40s, 60Fx30s, 72Fx25s, 90Fx20s 120Fx15s, 180Fx10s and 360Fx5s. The [4.47 – 30 mins] period, during which the phantom was motionless and the same number of disintegration theoretically occurred in the [0 – 30 mins] period, was used to generate static scans with and without (reference scan) motion correction and using the same framing parameters as above. Each static scan was reconstructed into a 344 × 344 × 127 element volume with a voxel size of 0.83 × 0.83 × 2.03 mm^3 using 3D Ordinary Poisson Ordered Subset Expectation Maximization reconstruction method with all corrections applied and using 3 iterations and 21 subsets. The image quality improvement (resp. the image quality degradation) resulting from the correction process was assessed by computing each time the nRMSE between images obtained from data that originally contained motion (resp. from the data that was originally motion-free) and the reference image. Note that in the case of the motion corrupted data, an estimate of the nRMSE due to differences that are caused by the noise only was subtracted to the measured nRMSE ($nRMSE_0$). Supplemental Figure 2 provides details about the employed method for estimating this value. Note that motion free images were obtained using the same portion of the original list mode as for the reference image and therefore this adjustment was not required.

Application to an actual ^{11}C-PIB study

119 patients: Mini Mental State Examination (MMSE) score = 22±5.7; age = 77±6; AD = 16%; NCI = 15%; MCI = 57; VAD = 12) underwent a 30 mins brain PET scan 40 mins post-injection of 370±10%MBq of ^{11}C-PIB. This human study was approved by the National Healthcare Group Domain Specific Review Board and written informed consent was obtained from all patients. Each list-mode data was rebinned into a single static frame during which motion correction was applied. Motion parameter estimates were measured from an initial reconstruction of the PET data using 90 frames of 20 secs and using the first 6 frames (120 secs) to create the target. The resulting volumes were

smoothed with a 3D Gaussian kernel of 16 mm (FWHM). Motion correction was performed using the normalization, data loss compensation as well as an oversampling factor of 3. These correction parameters were selected based on results obtained from the previous experiments. Motion and non-motion corrected scans were reconstructed using 3D Ordinary Poisson Ordered Subset Expectation Maximization reconstruction method with all corrections applied and using 3 iterations and 21 subsets. SUVR volumes were generated using the cerebellum grey matter as the reference region. Regional SUVR values for 12 Alzheimer specific regions were measured from the normalized volumes using the subject's parcellated structural MR images.

RESULTS

Rebinner accuracy

The $nRMS_0$ results reported in Figure 1 clearly indicated that data loss compensation (see the blue curves for rotations about X and Y), normalization (see rotation around Z - however blue and green curves are superimposed) as well as a minimum oversampling factor of 3 (see translations) are required for an accurate correction. An example of correction is shown in Figure 2 demonstrating visually the impact of a 10 mm motion along the Z axis as well as the contrast recovery achieved with the correction. Note that these results characterize only the accuracy of the correction when the exact motion parameters are used and do not account for inaccuracies in motion parameter estimates.

Accuracy of motion estimates

Accuracies in motion estimates reported in Figure 3A show that the higher the number of counts per frame the better the motion estimates. It is worth noting that registration led to better results with motion-free sinograms than when motion was present. Using the full statistics scan, a framing of 20 secs and a smoothing of 16 mm led to a registration errors of 0.41 and 0.85 mm without and with the presence of motion. Halving the injected dose or using a temporal sampling of 10 secs (LM50%_20s) increased the errors to 0.52 and 0.99 mm for the motion-free and motion-corrupted data respectively. Results shown in Figure 3A corresponds to inaccuracies caused by parameter estimates only, while

Figures 3B, 3C and 3D show the spatial resolution degradation as measured with the simulated point source, that is caused by both: inaccuracies in motion parameter estimates and by the rebinning process. We can see that an initial framing of 20 secs of the original scan (LM100%_20 secs) led to an average 1 mm increment in FWHM as compared to the motionless point source measurements (reference).

Hoffman study

Figure 4 shows the differences (nRMSE) between corrected and the reference images, when applied on motion corrupted data and motion free data. We can see that the correction applied on the motion corrupted data led to a decrease of the nRMSE from 16.7% (no correction) to less than 3%. In addition, when applied on motion free data, the correction process resulted in a nRMSE of less than 4%. Estimated motion from different framing configuration are given in Supplemental Figure 3. Supplemental Figure 4 shows reconstructed images before and after the correction.

Actual studies

An example of the correction on a actual ^{11}C-PIB scan involving large motion is shown in Figure 5, illustrating the improvement in contrast obtained with the correction. Figure 6 summarizes the motion observed during the correction of the ^{11}C-PIB scans. One can see that scans of subjects with low Mini-Mental State Exam (MMSE) contained higher level of motion than scans of subjects with normal MMSE (Fig. 6A), hinting that motion may affect unequally the different groups.

More than 29% and 9% of the scans with MMSE below 20 have undergone a mean absolute displacement across time of 5 and 10 mm respectively during the collection of the data. Still within the same group, in more than 56% (resp. 39%) of the scans, a displacement of at least 5 mm (resp. 10 mm) was observed at least once (Fig. 6B). As shown in Figure 6D, after 10 mins of acquisition, 43% (resp. 16% and 8%) of the scans suffered from displacements above 2 mm (resp. 5 mm and 10 mm). Figure 7 shows that the correction induced changes above 5% in more than 20% of the regional SUVR measurements.

DISCUSSION

In the current work, we proposed a novel event-by-event motion correction approach that is dedicated to the Siemens mMR machine. Our proposed implementation accounts for the sources of artefacts that have been identified in (*4*), namely: LOR discretization, differences in LOR normalization factors as well as data loss. Our results using the simulated ^{18}F-FDG scans with the well-controlled motions confirmed the importance of addressing them for an accurate correction. Each of these sources of error acts differently and with varying importance depending of the nature of the motion. From this study we found that a oversampling factor of 3 was sufficient as no significant improvement was obtained with a higher crystal sampling factor. We also aimed at finding the optimal trade-off between temporal frequency of the estimate (impacting the counting statistics within each frame) and motion estimates accuracy. We found that, in the case of our ^{11}C-PIB protocol, accurate motion parameters could be obtained every 20 secs, with mean errors of 0.41 mm when no motion was present and 0.85 mm with the presence of motion. Note that this optimization is specific to the spatial distribution and counting statistics of the ^{11}C-PIB data obtained with our protocol. Optimal registration and framing parameters should be re-evaluated for any other acquisition protocol and tracers. The corresponding resolution loss induced by motion estimate inaccuracies as well as by the rebinning process was on average below 1 mm and systematically below 1.5 mm (increase in FWHM). To the best of our knowledge, it is the first time that results on resolution loss induced by event-by-event rigid motion correction are reported. The Hoffman study mainly confirmed using an actual phantom scan the previous findings. The application of the correction method on the 119 actual ^{11}C-PIB scans led to the following observations: i) more than 21% of the scan were affected by a motion greater than 10 mm (39% for subjects with MMSE below 20) and ii), the correction of motion led to changes in Alzheimer-specific cortical regions of up to 30%, proving to be a great source of variability. Figure 7 indicates that the motion-induced biases cancels out (mean changes per region close to 0). However, it is not certain that this holds true if results were broken down by groups.

CONCLUSION

A list mode rebinner for the Siemens mMR scanner including rigid-body motion correction capability was developed and fully validated. It allows an accurate motion correction at a cost of minimal resolution reduction that is caused by inaccuracies in motion estimates as well as by the rebinning process. The application of the correction to a large cohort of ^{11}C-PIB scans confirmed the necessity to correct for motion for quantitative results.

REFERENCES

1. Fayad H, Lamare F, Merlin T, Visvikis D. Motion correction using anatomical information in PET/CT and PET/MR hybrid imaging. *Q J Nucl Med Mol Imaging*. 2016;60:12–24.

2. Costes N, Dagher A, Larcher K, Evans A C, Collins D L, Reilhac A. Motion correction of multi-frame PET data in neuroreceptor mapping: simulation based validation. *Neuroimage*. 2009;47:1496–1505.

3. Menke M, Atkins M S, Buckley K R. Compensation methods for head motion detected during PET imaging. *IEEE Trans Nucl Sci*. 1996;43:310–317.

4. Bühler P, Just U, Will E, Kotzerke J, Van den Hoff J. An accurate method for correction of head movement in PET. *IEEE Trans Med Imaging*. 2004;23:1176–1185.

5. Rahmim A, Dinelle K, Cheng J-C, et al. Accurate event-driven motion compensation in high-resolution PET incorporating scattered and random events. *IEEE Trans Med Imaging*. 2008;27:1018–1033.

6. Catana C, Benner T, Van der Kouwe A, Byars L, et al. MRI-assisted PET motion correction for neurologic studies in an integrated MR-PET scanner. *J Nucl Med*. 2011;52:154–161.

7. Ullisch M G, Scheins J J, Weirich C, et al. MR-based PET motion correction procedure for simultaneous MR-PET neuroimaging of human brain. *PloS ONE*. 2012;7:e48149.

8. Delso G, Fürst S, Jakoby B, et al. Performance measurements of the Siemens mMR integrated whole-body PET/MR scanner. *J Nucl Med*. 2011;52:1914–1922.

9. Panin V Y, Kehren F, Michel C, Casey M. Fully 3-D PET reconstruction with system matrix derived from point source measurements. *IEEE Trans Med Imaging*. 2006;25:907–921.

10. Vincent R D, Neelin P, Khalili-Mahani N, et al. MINC 2.0: a flexible format for multi-modal images. *Front Neuroinform*. 2016;11:10-35.

11. Reilhac A, Sjoholm T, Thomas B A, et al. Validation and application of PET-SORTEO for the geometry of the Siemens mMR scanner. *PSMR. Conference.*, Cologne, Germany, 2016.

12. Lartizien C, Aubin J-B, Buvat I. Comparison of bootstrap resampling methods for 3-D PET imaging. *IEEE Trans Med Imaging*. 2010;29:1442–54.

13. National Electrical Manufacturers Association. NEMA standards publication NU 2–2007, performance measurements of positron emission tomographs. 2007. Rosslyn, VA. 26–33.

Figure 1

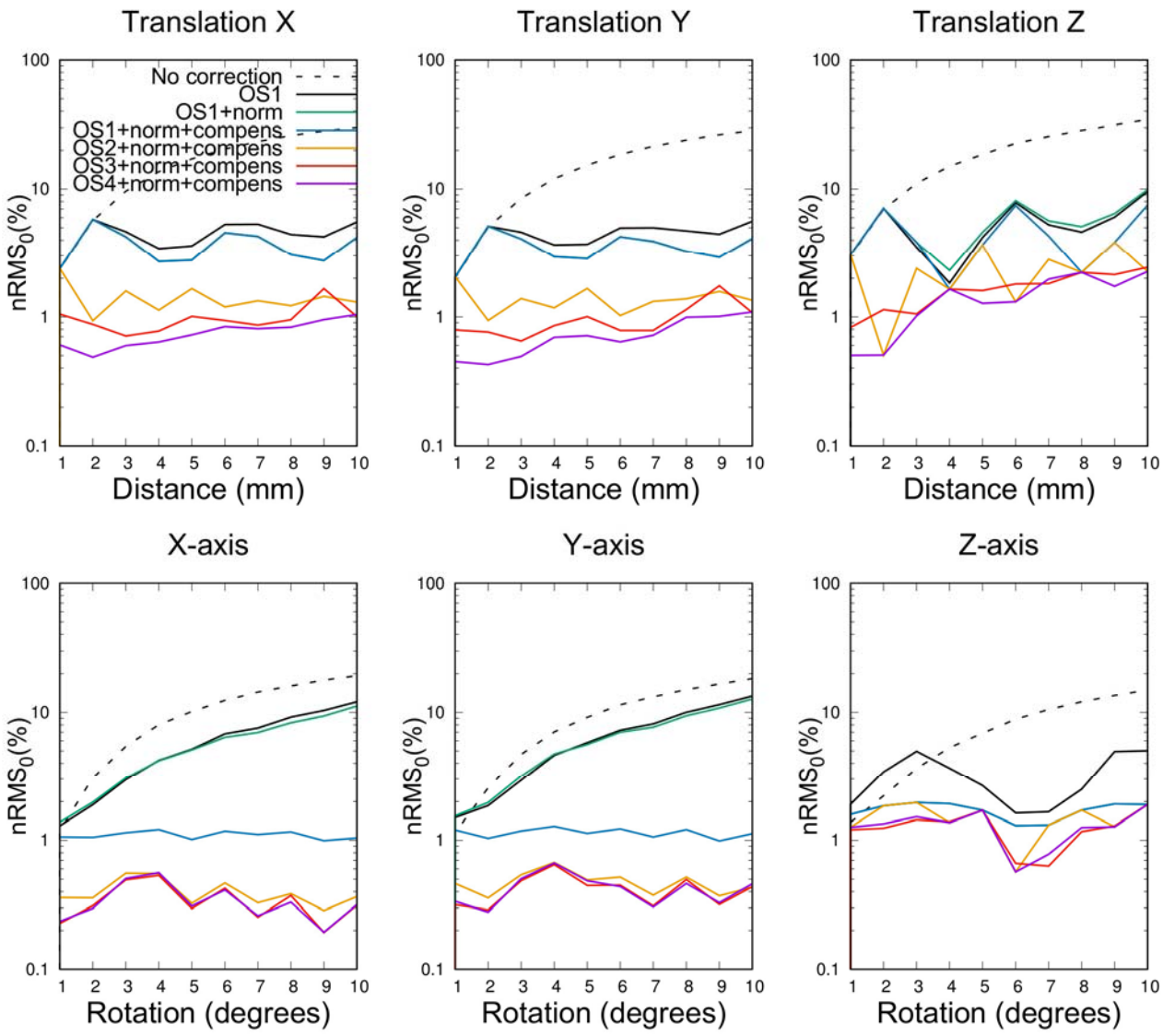

Figure 1: $nRMS_0$ error (%) computed between the corrected and reference volumes as a function of the magnitude of the motion and for different correction parameters: simple line approach (oversampling of 1 = OS_1), OS_1 including normalization (OS_1+norm), OS_1+norm with data loss compensation (OS_1+norm+compens) and different levels of crystal oversampling (2, 3 and 4). $nRMS_0$ obtained when no correction was applied is also shown for comparison. For clarity, only results obtained with positive motion are shown.

Figure 2

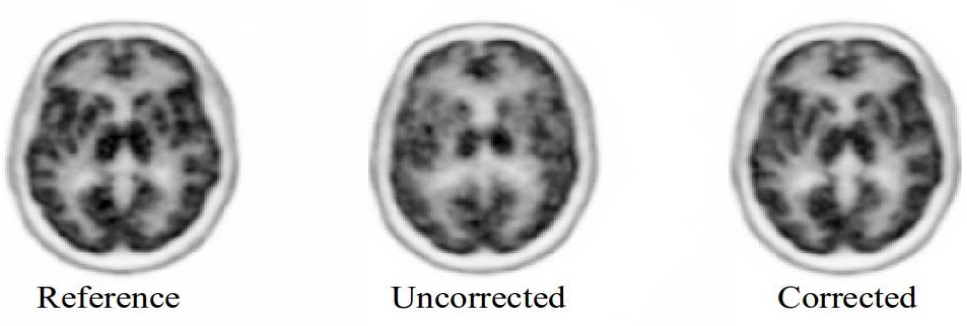

Figure 2: Uncorrected and corrected simulated ^{18}F-FDG images reconstructed from the scan with a 10 mm translation along the Z axis. Normalization, data loss compensation as well as an oversampling factor of 3 was used for the correction. The simulated reference volume is also shown for comparison.

Figure 3

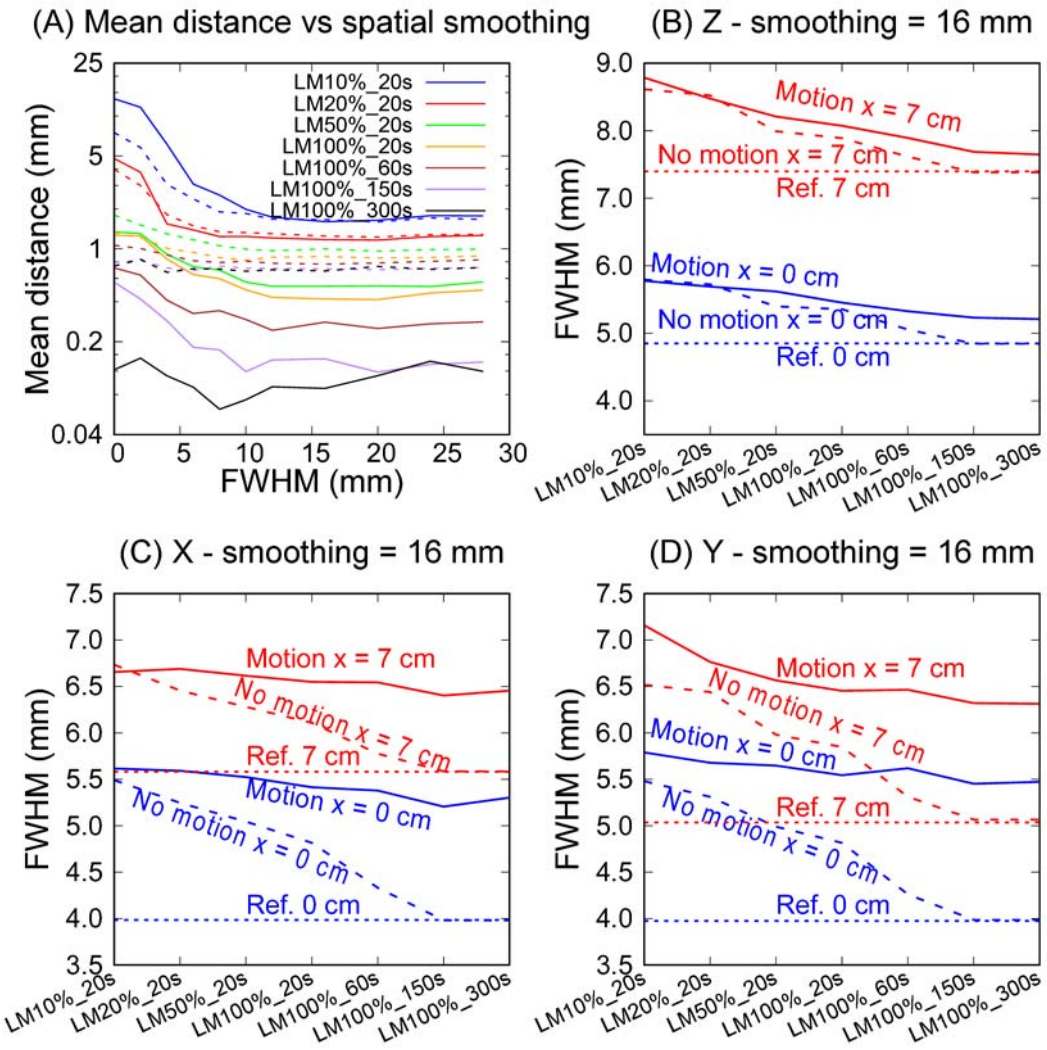

Figure 3: (A): Mean absolute displacements across time of a point located at a radial distance of 7 cm in the central transverse plane caused by inaccuracies in motion parameter estimates as a function of the Gaussian smoothing. Displacements obtained from the 7 motion-free sinograms are in solid line, while results obtained with the motion corrupted data are shown in dashed line with matching color code.(B-D): Spatial resolution degradation resulting from the whole correction process (inaccuracies in motion parameter estimates and resolution loss due to the rebinning) as a function of the counting statistics. "Motion" (resp. "No motion") refers to the situation where the point source was rebinned using the motion parameters measured from the motion corrupted (resp. Motion free) ^{11}C-PIB data. The reference spatial resolutions measured at the center (ref. 0 cm) as well at an radial offset of 7 cm (ref. 7 cm) are also shown for comparison".

Figure 4

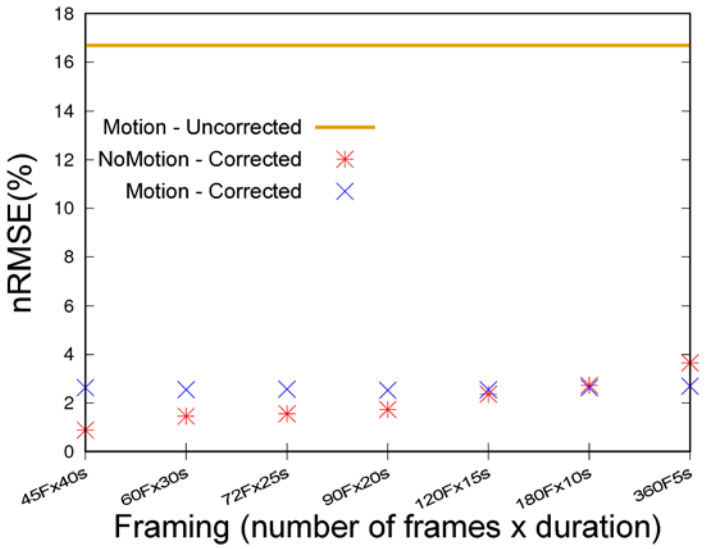

Figure 4: nRMSE(%) computed between the corrected and the reference images, when applied on motion corrupted data (motion – corrected) and motion free (no motion – corrected) data. The nRMSE computed between the motion uncorrected corrupted scan and the reference scan is also shown for comparison.

Figure 5

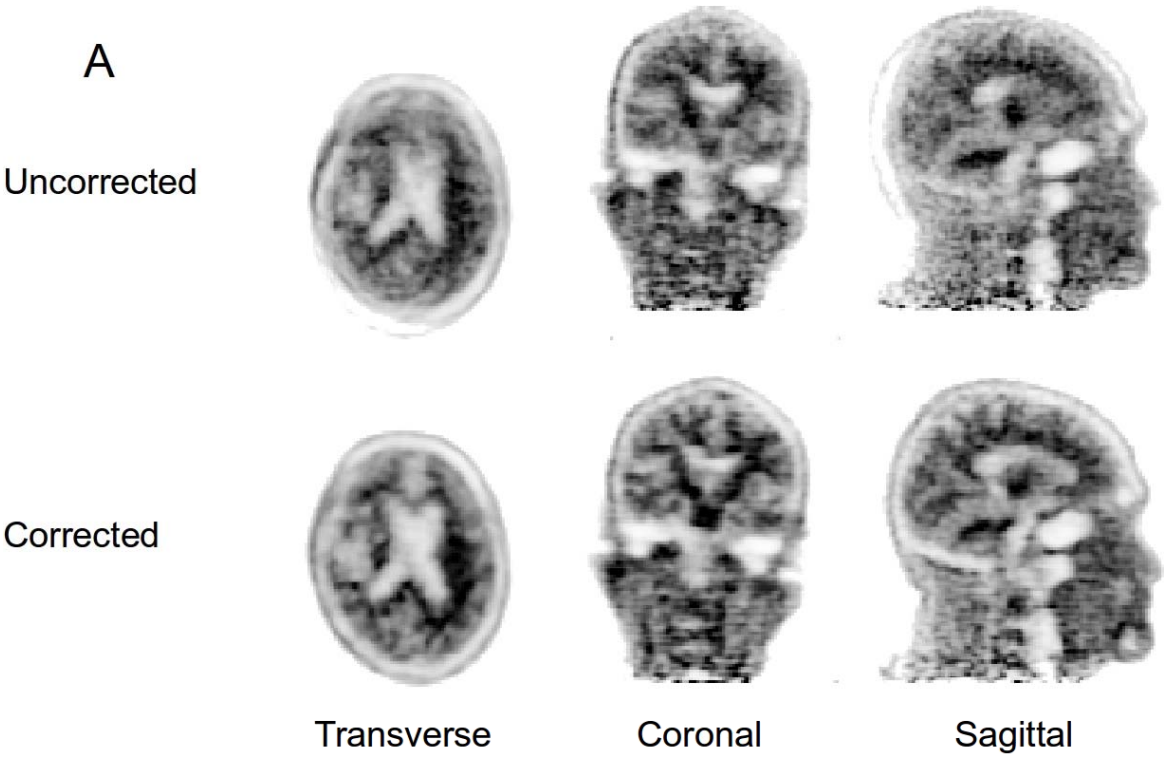

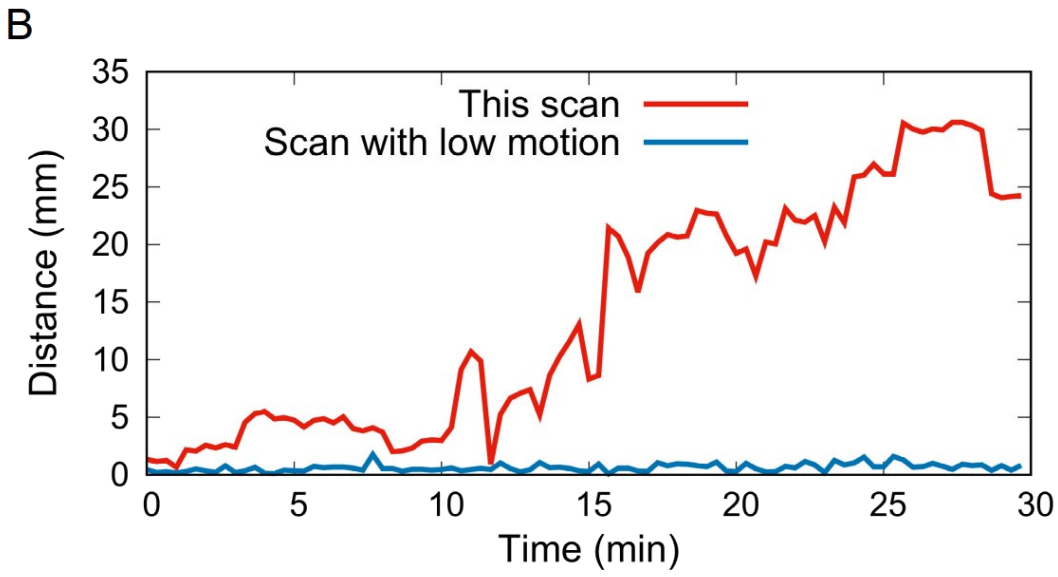

Figure 5: (A) Uncorrected and corrected 30 mins ^{11}C-PIB study with large motion. (B) corresponding displacements undergone by a point located at 7 cm radially as a function of time. The displacement curve obtained from a scan with low level of motion is also shown for comparison.

Figure 6

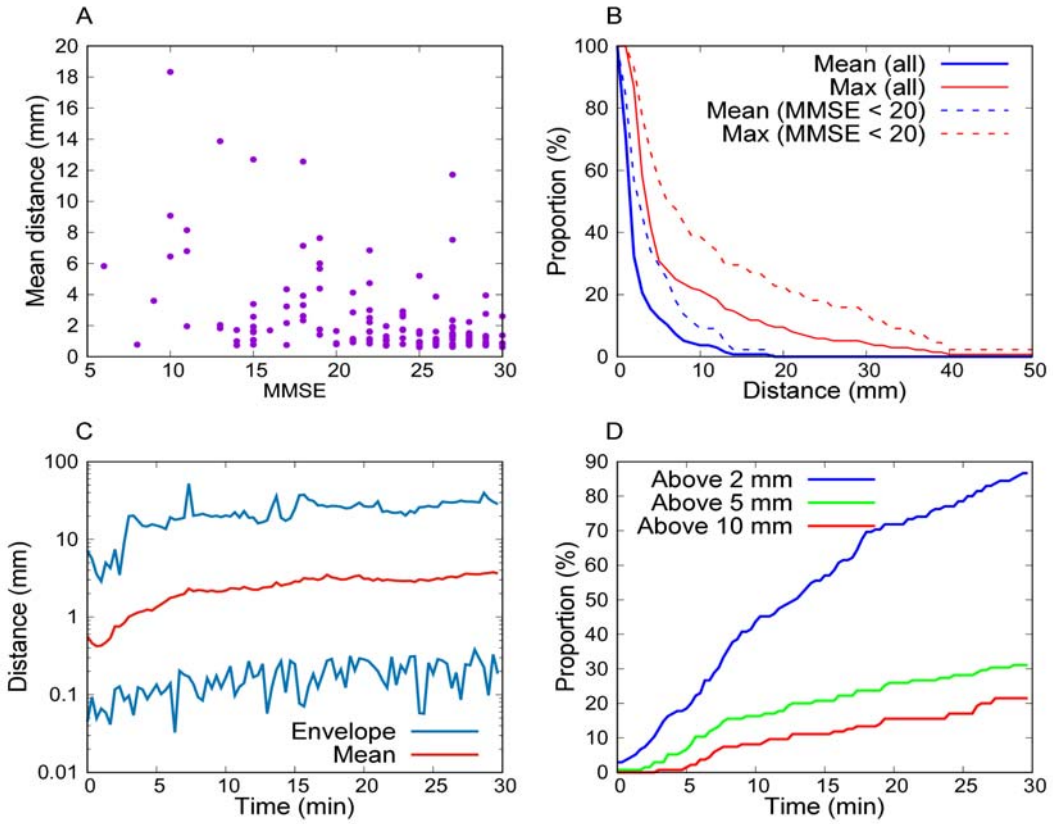

Figure 6: Description of the motion measured from the 119 ^{11}C-PIB scans. (A) Mean head displacement over time as a function of subject MMSE. (B) Proportion of scans whose mean (blue) and max (red) displacements computed over the scan duration were above the distance given in X-axis. (C) Mean (and envelope) displacement curves across time. (D) Proportion of scans with displacement above 2 mm (blue), 5 mm (green) and 10 mm (red) as a function of time. In all graphs, displacements were computed for a point located in the central plane and at a radial distance of 7 cm on the X axis.

Figure 7

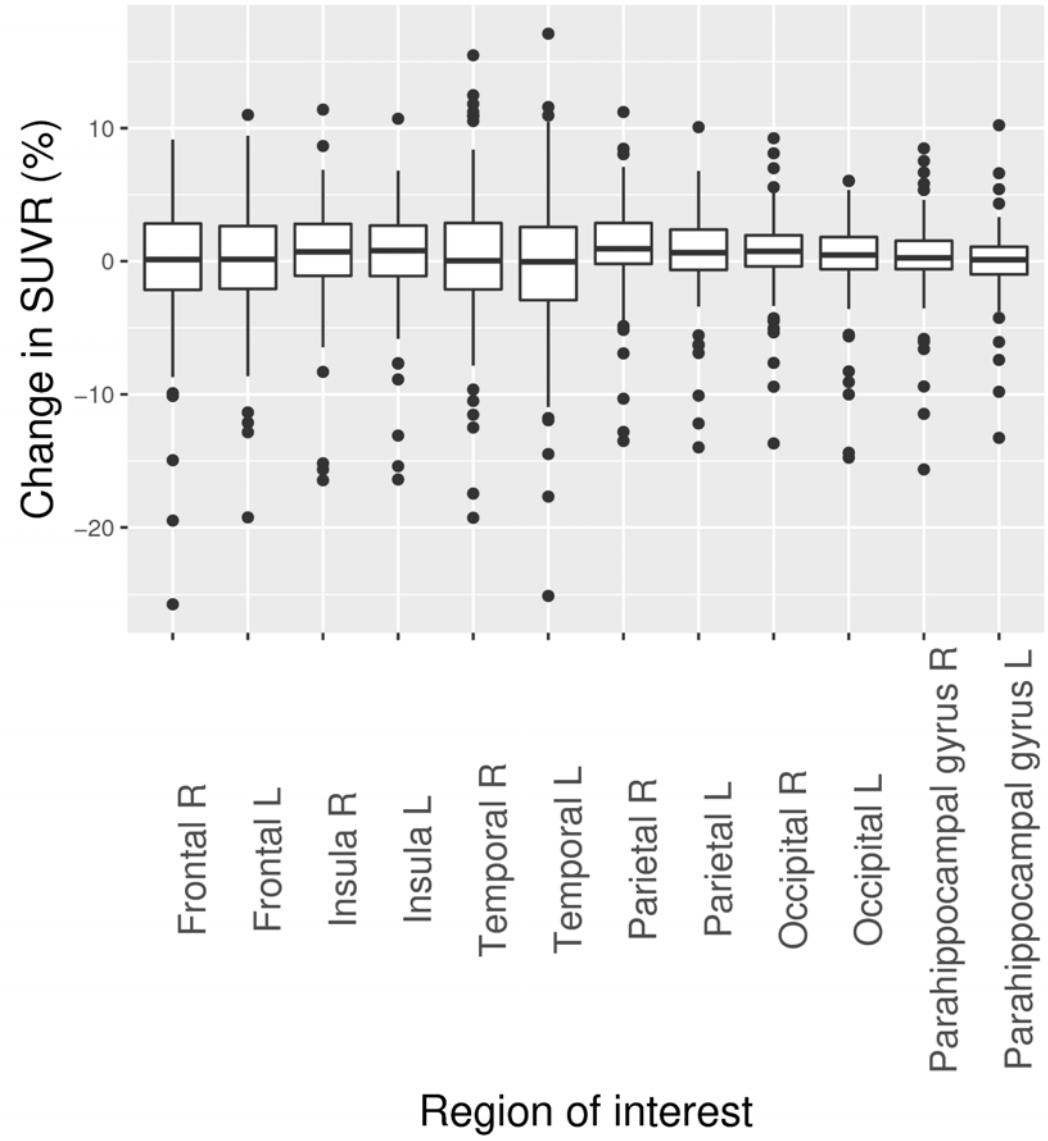

Figure 7: Changes in SUVR obtained with the correction and for different cortical ROIs.

Table 1: Description of the motion free and motion corrupted sinograms

Data scan	Frames	Duration (secs)	Total prompts	Net trues in [1st – last] frames
LM10%_20s	90	20	13M	63k-173k
LM20%_20s	90	20	27M	126k-346k
LM50%_20s	90	20	67.7M	316k-865k
LM100%_20s	90	20	135.5M	870k-2.39M
LM100%_60s	30	60	135.5M	1.91M-5.13M
LM100%_150s	12	150	135.5M	4.91M-12.5M
LM100%_300s	6	300	135.5M	10.25M-24M

Table 2: Motion parameters used for the generation of the motion-corrupted sinograms

Times (secs)	Tx (mm)	Ty (mm)	Tz (mm)	Rx (degrees)	Ry (degrees)	Rz (degrees)
300	0	2	0	0	0	2
600	2	-5	0	0	0	-5
900	4	5	0	0	0	5
1200	-4	-10	0	0	0	7
1500	4	10	0	0	0	-7

Supplemental Figure 1:

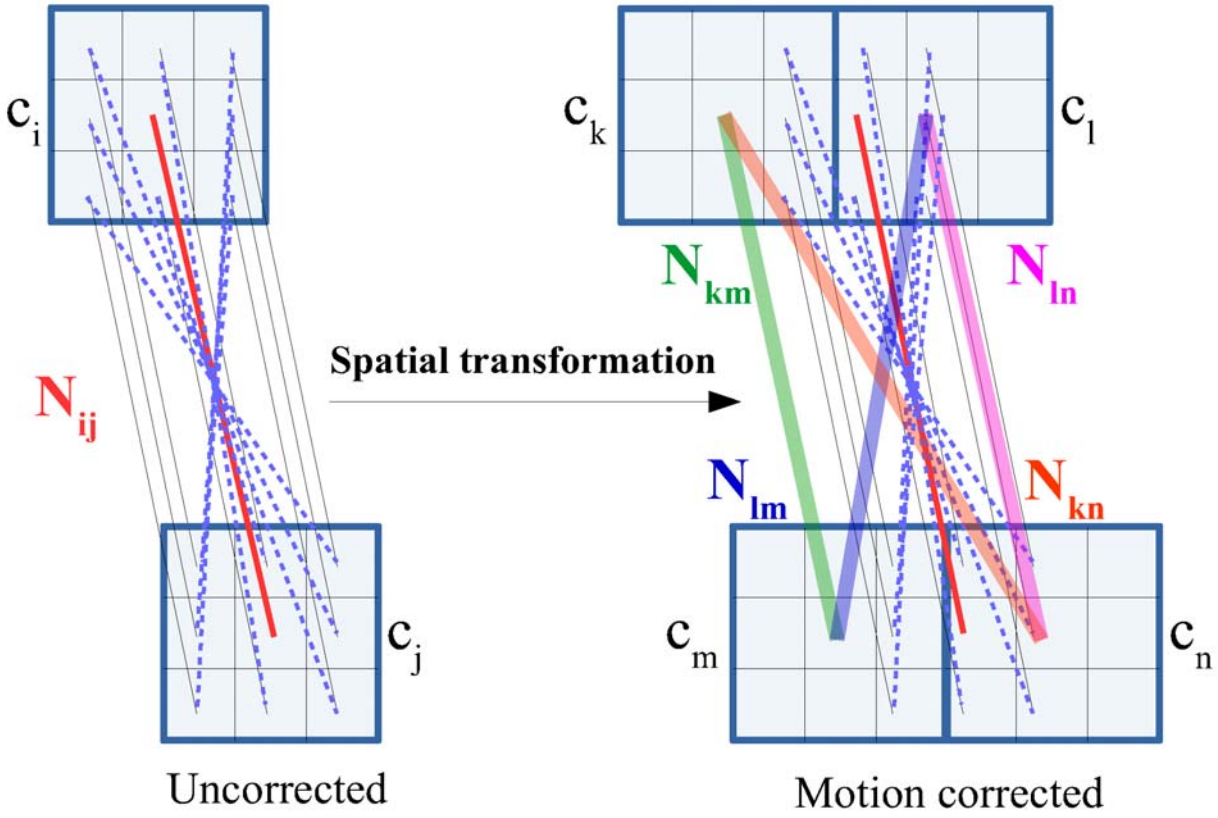

Supplemental Figure 1: Illustration of the rebinning process. M events detected within the LOR joining crystals C_i and C_j are to be reassigned to the correct LORs using the registration parameters. The M counts are first normalized by the normalization factor corresponding to the original LOR_{ij} ($M.N_{ij}$). Each crystal is then divided in 3x3 sub-crystals (OS_3), leading to 9 direct (black) and 8 oblique (dash blue) sub-crystal combinations. The distribution of the M counts onto the correct LORs is done by applying the spatial transformation on each of the lines and by computing the proportion falling into each LOR. In this example, 3/17, 8/17, 3/17 and 3/17 of the events are re-assigned to LOR_{km}, LOR_{ln}, LOR_{kn} and LOR_{lm} respectively. The unnormalized value to be assigned to each new LOR (LOR_{ln} here) is then $8.M.N_{ij}/(17.N_{ln})$. Note that if no oversampling was used (OS_1), the application of the spatial transformation to the central line (the red line) would have led to the assignment of all the counts to LOR_{ln}.

Supplemental Figure 2:

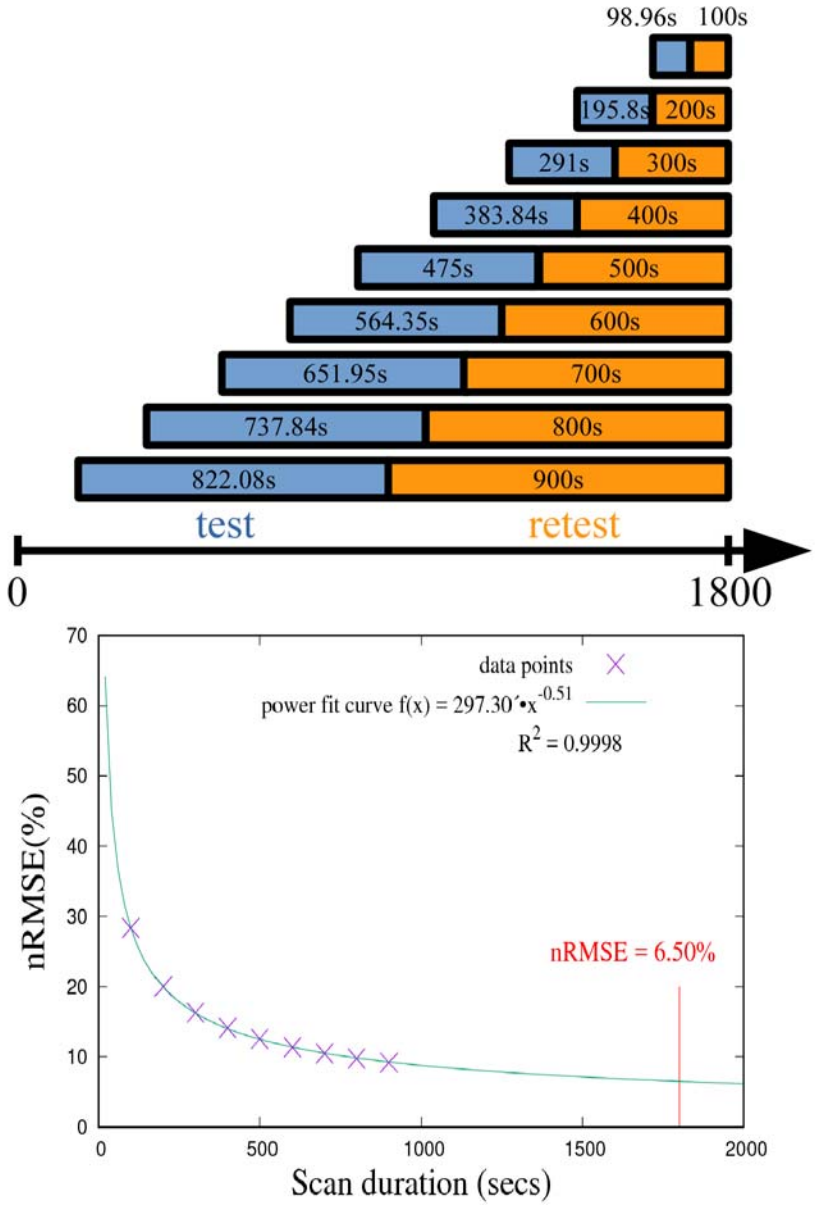

Supplemental Figure 2: Estimation of the noise contribution to the nRMSE measurements. The portion of the list mode data during which the phantom was motionless [0 – 30 mins] was divided in successive test and retest scans with duration for the retest scans going from 100 secs to 900 secs by step of 100 secs. Note that the frame durations of the corresponding test scans were slightly reduced so that the same theoretical number of disintegrations occurred during both scans. The nRMSE(%) was computed between each test-retest scan pair and plotted as a function of the scan duration. The data was fitted with a power curve leading to the following equation: $nRMSE(t) = 297.3 \cdot t^{-10.51}$ ($R^2 = 0.9998$). The extrapolation to a 30 mins acquisition scan led to an estimated RMSE of 6.5% that is purely caused by noise.

Supplemental Figure 3:

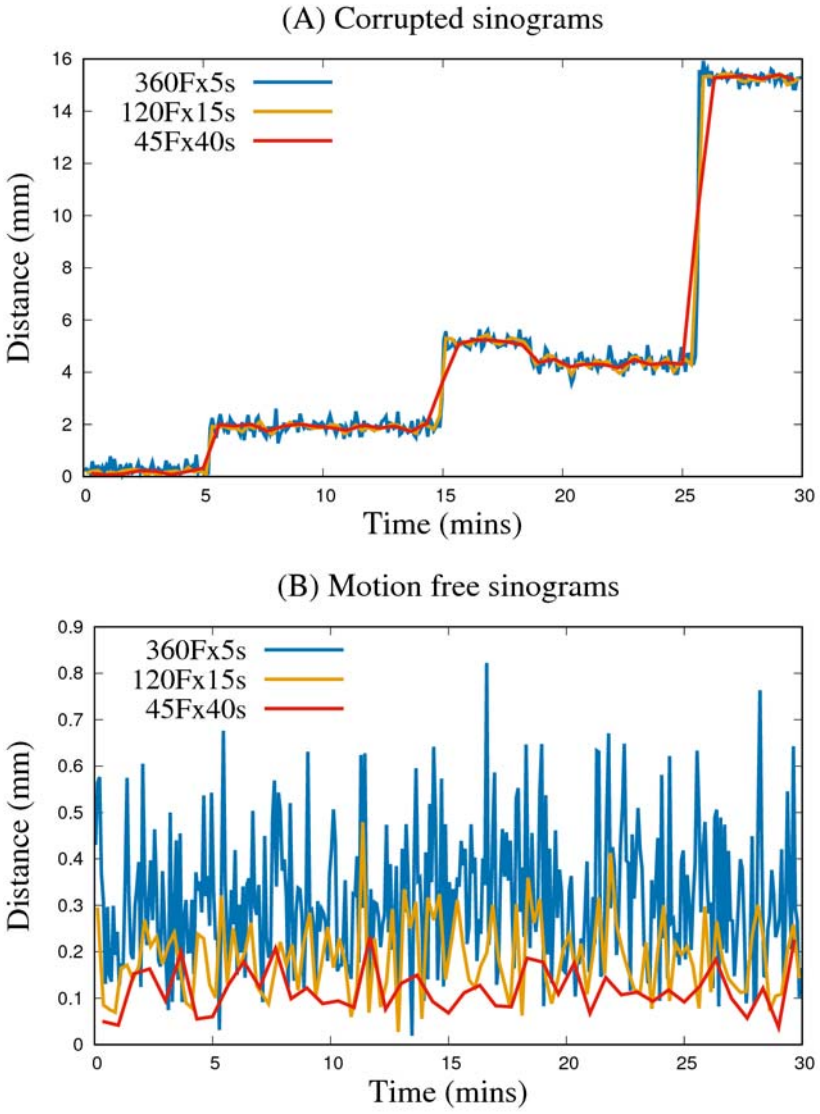

Supplemental Figure 3: Motion across time that was estimated using 3 different framing: 45 frames of 40 secs each (45Fx40s), 120 frames of 15 secs each (120Fx15s) and 360 frames of 5 secs each (360Fx5s). Each time a Gaussian blurring of 16 mm (FWHM) was applied on the image prior the motion parameter estimation. Motion are expressed in mm and for a point source located at a radial distance of 7 cm in the central transverse plane. (A) Original data contained motion (second part of the list-mode acquisition). (B) Original data were motion free (first part of the scan). The counting statics in each frame of the 120Fx15s (resp. 360Fx5s) scans roughly correspond to the counting statistic at in the early frames (resp. last frames) of the ^{11}C-PIB scans.

Supplemental Figure 4:

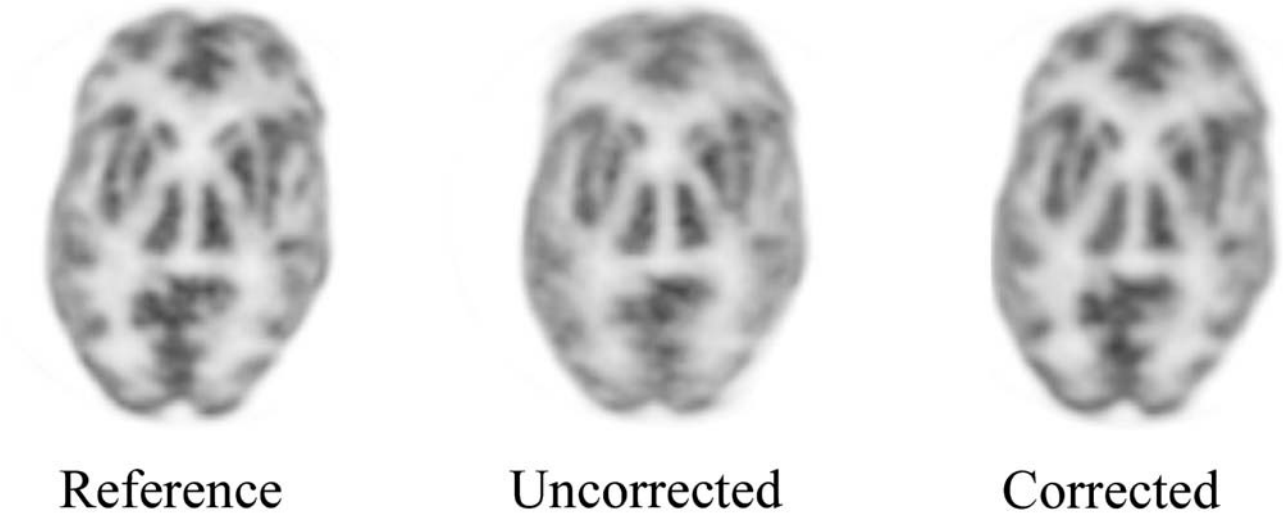

Supplemental Figure 4: Reference, uncorrected, corrected images reconstructed from the Hoffman phantom scan. Motion parameters were estimated from an initial volume containing 120 frames of 15 secs each.